Supplemental Information

Sn-assisted heteroepitaxy improves $ZnTiN_2$ photoabsorbers

John S. Mangum[1,*], Sijia Ke[2,3], Melissa K. Gish[1], Emily K. Raulerson[1], Craig L. Perkins[1], Jeffrey B. Neaton[4,5,6], Andriy Zakutayev[1], Ann L. Greenaway[1,*]

[1]Materials Chemical and Computational Science Directorate, National Renewable Energy Laboratory, Golden, Colorado 80401, USA
[2]Department of Materials Science and Engineering, University of California Berkeley, Berkeley, California 94720, USA
[3]Chemical Sciences Division, Lawrence Berkeley National Laboratory, Berkeley, California 94720, USA
[4]Department of Physics, University of California at Berkeley, California 94720, USA
[5]Materials Sciences Division, Lawrence Berkeley National Laboratory, Berkeley, California 94720, USA
[6]Kavli Energy Nanosciences Institute at Berkeley, Berkeley, California 94720, USA
[*]corresponding authors: John.Mangum@nrel.gov, Ann.Greenaway@nrel.gov

Supplemental Table 1. Deposition parameters for $ZnTiN_2$ films.

Sample ID	**Substrate**	T_{sp} **[°C]**	**Base Pressure [Torr]**	**Zn Power [W]**	**Zn (5% Sn) Power [W]**	**Ti Power [W]**	**ZnTi Power [W]**	$\frac{Sn}{(Sn+Zn+Ti)}$
$ZnTiN_2$-AT-Si	silicon	ambient (~25)	2.9×10^{-7}	--	--	100	150	--
$ZnTiN_2$-AT-EXG	EXG glass	ambient (~25)	0.9×10^{-7}	--	--	100	150	--
$ZnTiN_2$-AT-sapph	sapphire	ambient (~25)	2.5×10^{-7}	--	--	100	150	--
$ZnTiN_2$-300C-sapph	sapphire	300	1.8×10^{-7}	50	--	--	150	--
Sn:$ZnTiN_2$-300C-sapph	sapphire	300	2.0×10^{-7}	--	40	--	150	~12%

(a) ZnTiN$_2$ on Si, T_{sp} = ambient

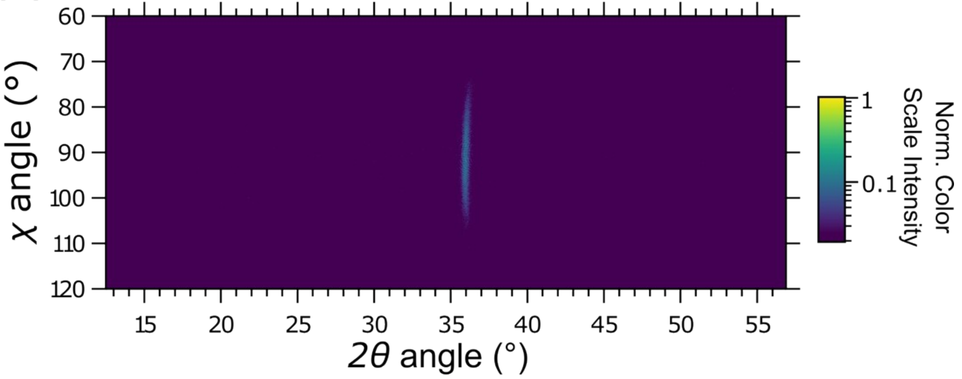

(b) ZnTiN$_2$ on sapphire, T_{sp} = ambient

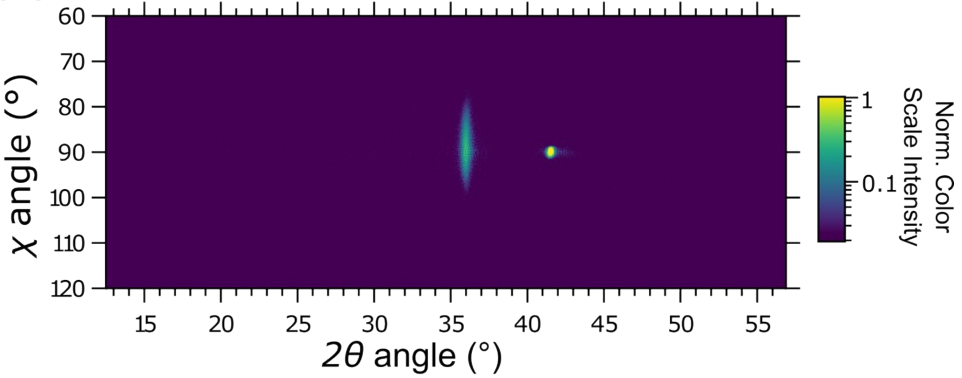

(c) ZnTiN$_2$ on sapphire, T_{sp} = 300 °C

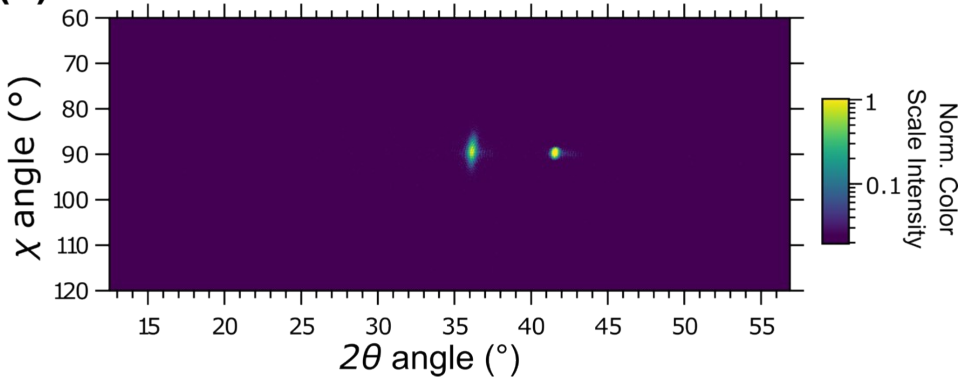

Supplemental Figure 1. 2D XRD plots across the entire measured range corresponding to the plots shown in Figure 1.

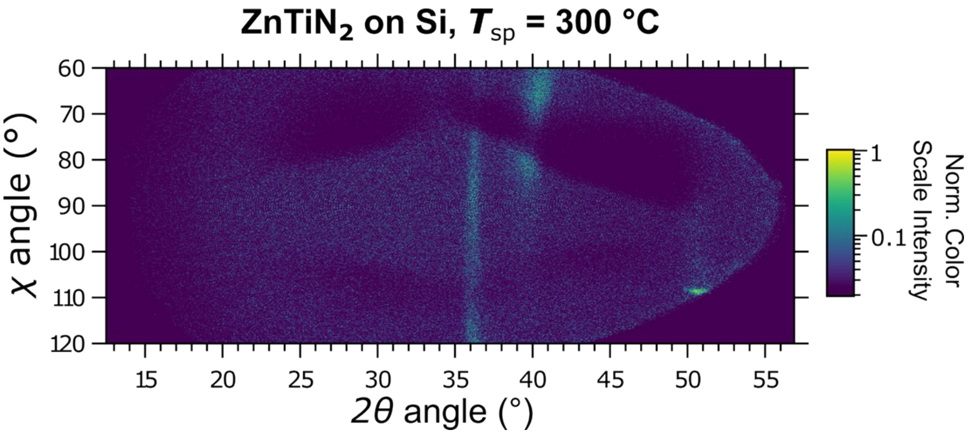

Supplemental Figure 2. 2D XRD plot measured from a ZnTiN$_2$ film grown on Si at 300 °C.

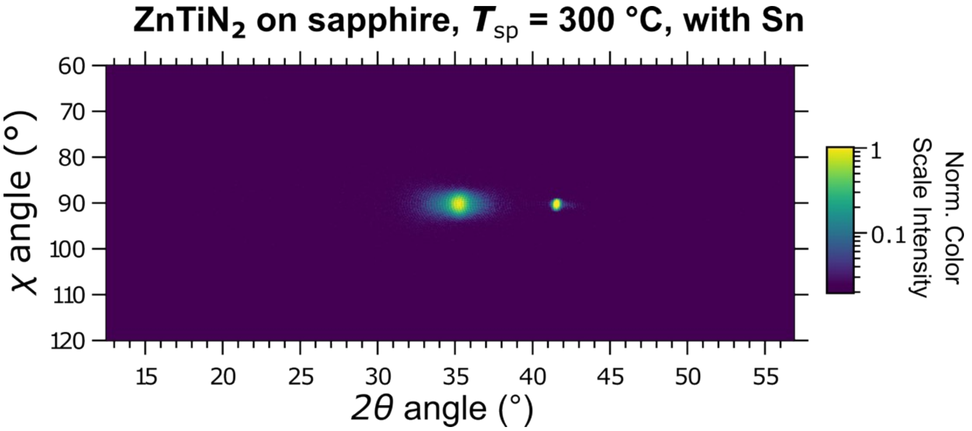

Supplemental Figure 3. 2D XRD plot measured from a Sn:ZnTiN$_2$ film grown on sapphire at 300 °C.

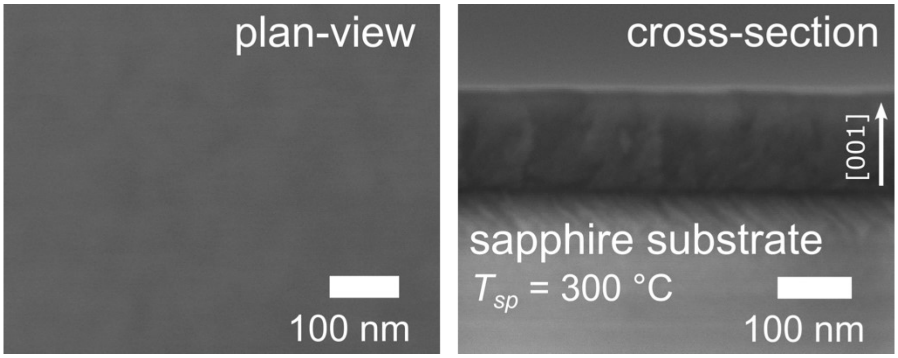

Supplemental Figure 4. (left) Plan-view and **(right)** cross-sectional SEM micrographs of a Sn:ZnTiN$_2$ film grown on sapphire at 300 °C.

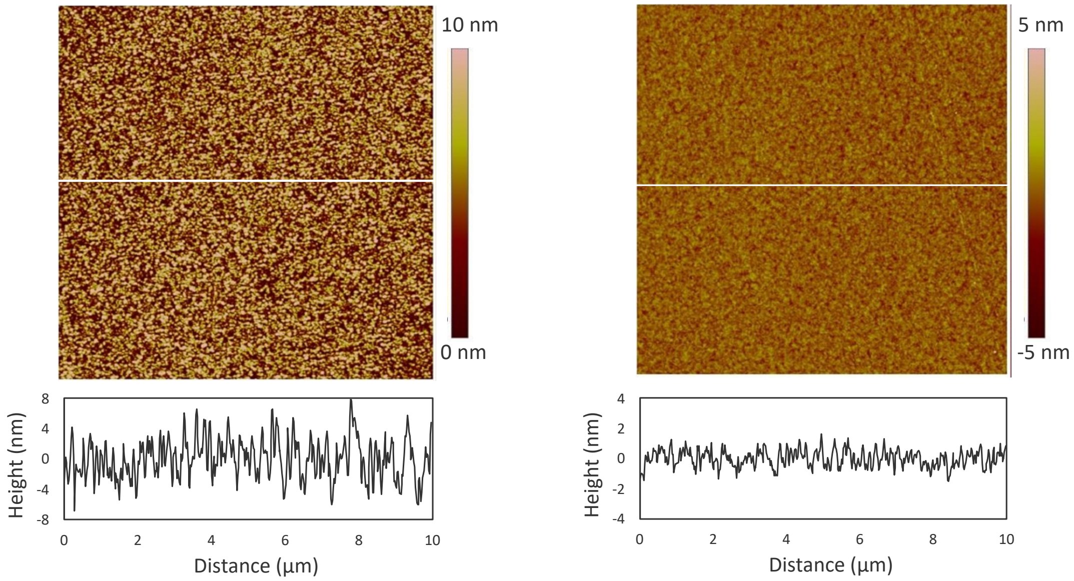

Supplemental Figure 5. 10 µm x 10 µm AFM maps and corresponding line profiles indicated by white line for **(left)** $ZnTiN_2$ film grown on sapphire at 300 °C ($R_{RMS} \approx 3.00$ nm) and **(right)** Sn:$ZnTiN_2$ film grown on sapphire at 300 °C ($R_{RMS} \approx 0.55$ nm).

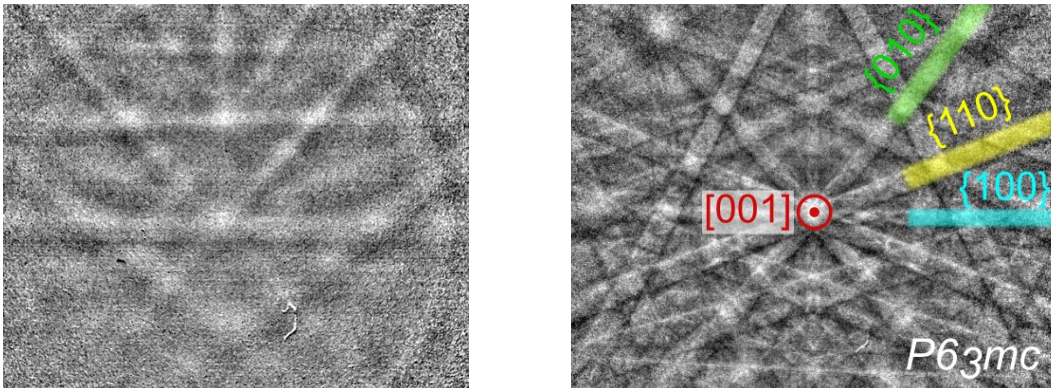

Supplemental Figure 6. EBSPs from **(left)** $ZnTiN_2$ film grown on sapphire at 300 °C and **(right)** Sn:$ZnTiN_2$ film grown on sapphire at 300 °C (same as Figure 3c).

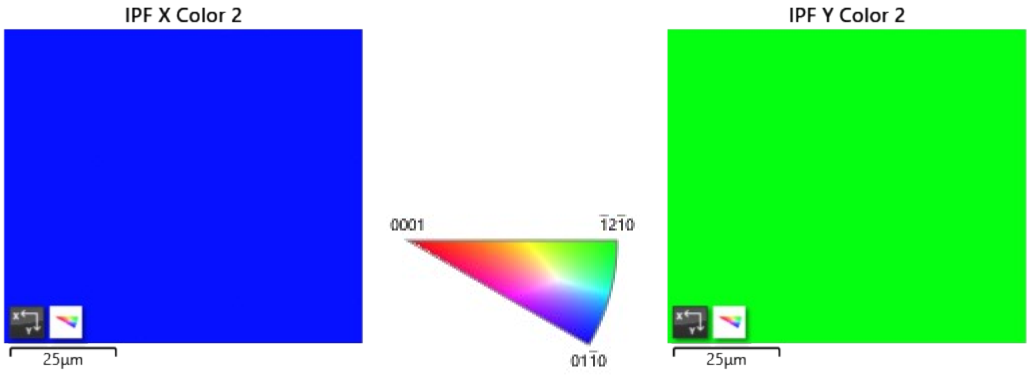

Supplemental Figure 7. EBSD IPF maps for **(left)** X-axis and **(right)** Y-axis that correspond to the IPF Z-axis map shown in Figure 3a.

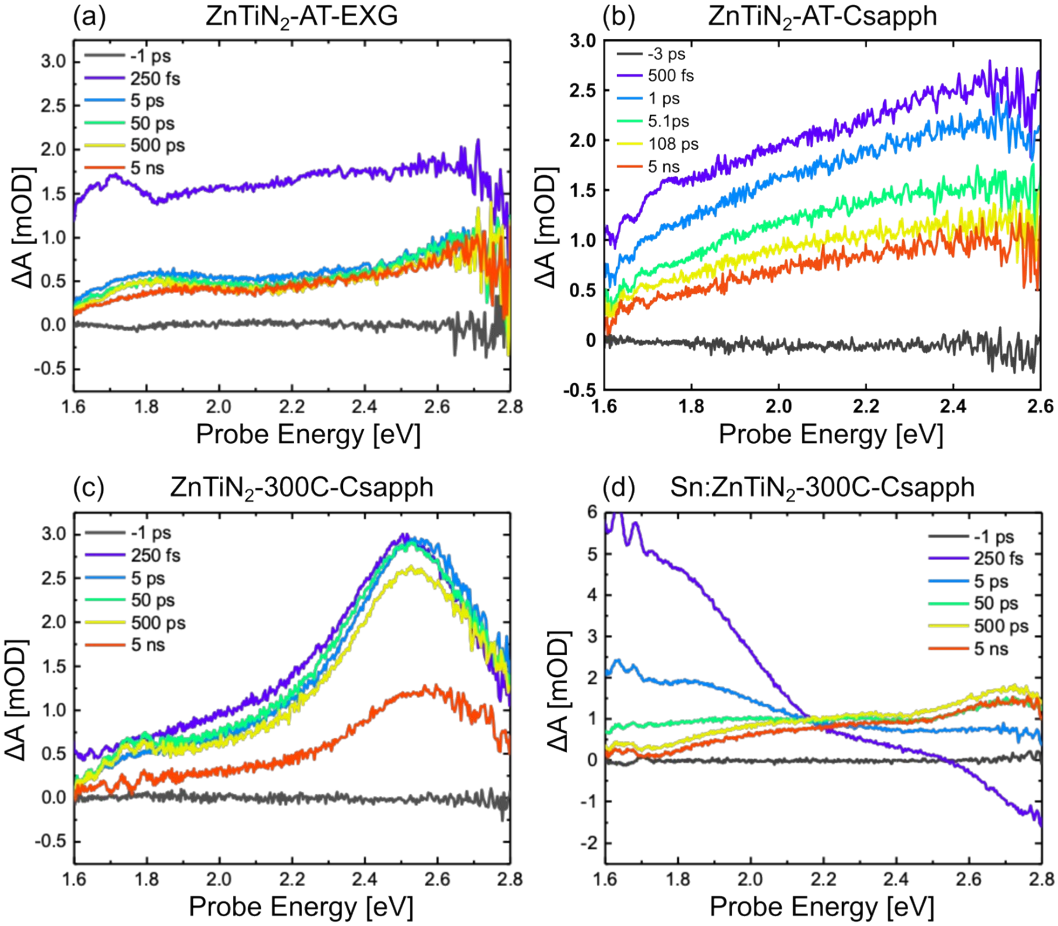

Supplemental Figure 8. Full transient absorption spectra corresponding to the films shown in Figure 4b.

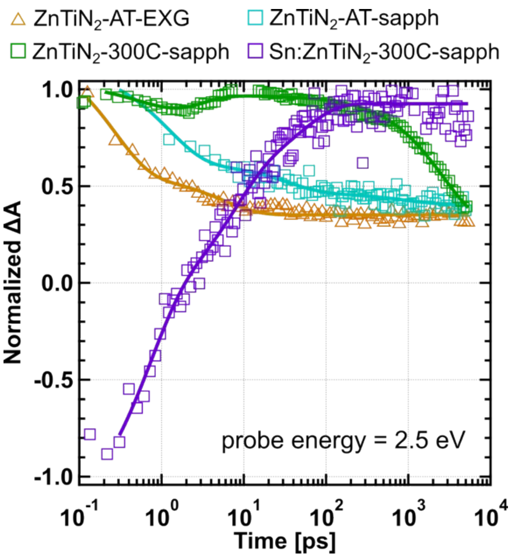

Supplemental Figure 9. Transient absorption kinetics of films grown with varying growth conditions at a probe energy of 2.5 eV after photoexcitation at 3.1 eV, which is more sensitive to the kinetics of trapped photoexcited charge carriers. Normalized TA kinetic data are shown as markers and fits as solid lines. The $ZnTiN_2$-300C-sapph film 2.5 eV kinetic data reaches a maximum after a few ps, followed by a significant decay after 1 ns. The similar trends observed in the 1.8 eV and 2.5 eV kinetic data for the $ZnTiN_2$-300C-sapph film suggest an abundance of carrier trap states across the probed energy range, consistent with its high carrier concentration. In contrast, the Sn:$ZnTiN_2$-300C-sapph film grows to a maximum at around 100 ps and shows only a minor decay signature after a few ns. The later onset of carrier trapping and more gradual kinetic decay observed in the Sn:$ZnTiN_2$-300C-sapph film, combined with its more typical exponential decay signature at 1.8 eV, suggests a different mechanism where carriers transition from their initial excited states to longer lived trap states before eventually recombining on the ns time scale.

Supplemental computational details:

Supplemental Figure 10 shows our calculated site-projected density of states, indicating the inverse participation ratio, which quantifies the degree of localization of the wavefunction on each site at each energy. We introduce one Sn cation into two cation-ordered 2x2x2 supercells, each containing a total of 128 atoms, with Sn substituting one Zn (**Supplemental Figure 10a**) in one case and Sn substituting one Ti (**Supplemental Figure 10b**) in the other case (1.6% of cation sites). The density of states is mostly unchanged when Sn substitutes for Ti in this supercell compared to the supercell without Sn. However, a deep gap state localized at the Sn defect appears when Sn is substituted for Zn. This is in contrast to optical measurements, from which it can be inferred that Sn-containing $ZnTiN_2$ films possess fewer mid-gap states.

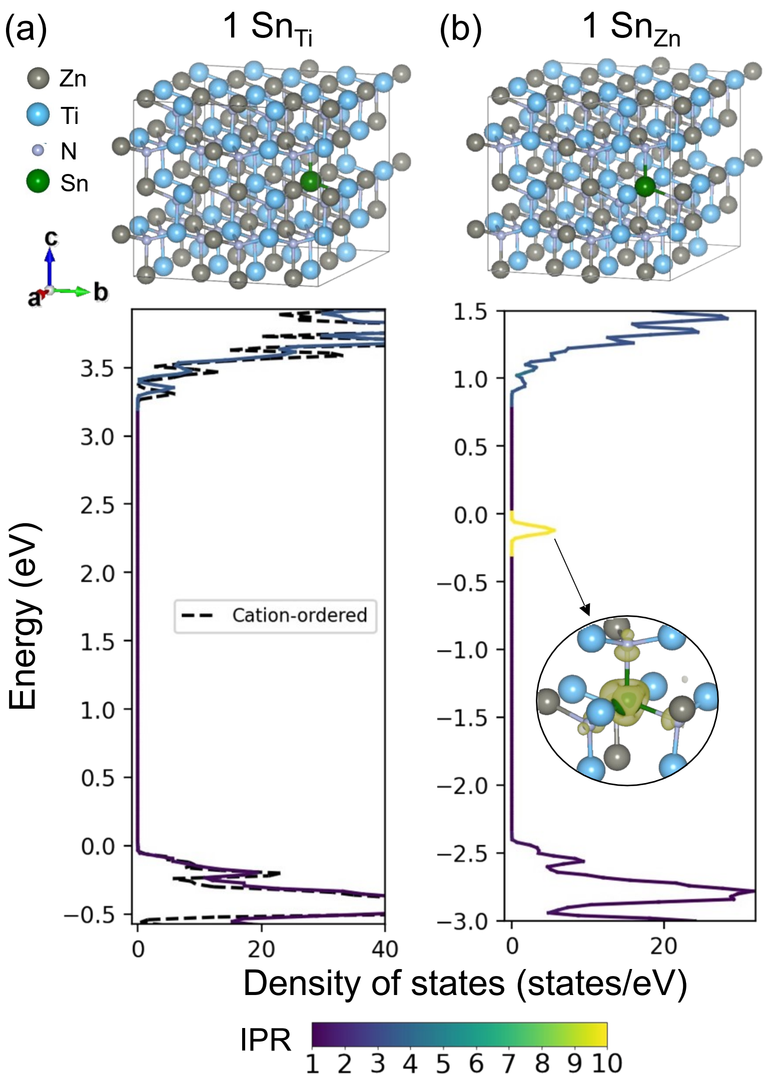

Supplemental Figure 10. Projected density of states of cation-ordered $ZnTiN_2$ supercells with 1.6% **(a)** Sn_{Ti} and **(b)** Sn_{Zn}. The inverse participation ratio is displayed on a color scale. The inset of (b) shows the charge density of the in-gap state, localizing on Sn_{Zn}.

The construction of the cation-disordered supercell used here is the same as the Supercell R* in Supplemental Reference 1. We first use quasi-random numbers to determine cation occupation to create one randomly distributed cation-disordered supercell, then we apply extra quasi-random Zn-Ti swaps to remove existing N-Zn_4Ti_0 and increase the octet-rule-obeying N-Zn_2Ti_2 motif density inside the random supercell, which gives us Supercell R* used in this work. The removal of N-Zn_4Ti_0 and the increase of N-Zn_2Ti_2 is to reduce the formation energy penalties.

We introduce one Sn cation into the cation-disordered 2x2x2 supercell (Supercell R*), each containing a total of 128 atoms, with one Sn substituting one Zn or one Ti (1.6% of cation sites). For Zn or Ti sites with a certain number of Zn neighbors, we randomly choose one site to calculate the formation energy. The relative formation energy plots are shown in **Supplemental Figure 11** with the smallest formation energy set as the reference.

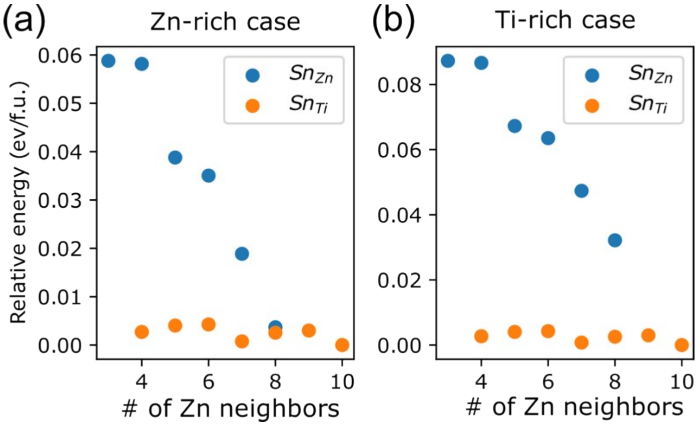

Supplemental Figure 11. Relative formation energy versus Sn substitution in two extreme chemical environments under different chemical potentials, within the $ZnTiN_2$ phase space, **(a)** Zn has the lowest chemical potential ($\mu_{Zn} = \mu^0_{Zn}$- 0.322 eV) and Ti has the highest chemical potential ($\mu_{Ti} = \mu^0_{Ti}$ - 3.472 eV) **(b)** Zn has the highest chemical potential ($\mu_{Zn} = \mu^0_{Zn}$ - 0 eV) and Ti has the lowest chemical potential ($\mu_{Ti}= \mu^0_{Ti}$ - 4.062 eV) , where μ^0_{Zn} and μ^0_{Ti} are DFT-PBE calculated energy for metal Zn and Ti, the relative chemical potential within $ZnTiN_2$ phase is obtained from materials project.[2,3] The reference zero is chosen to be the lowest formation energy for all supercells we consider.

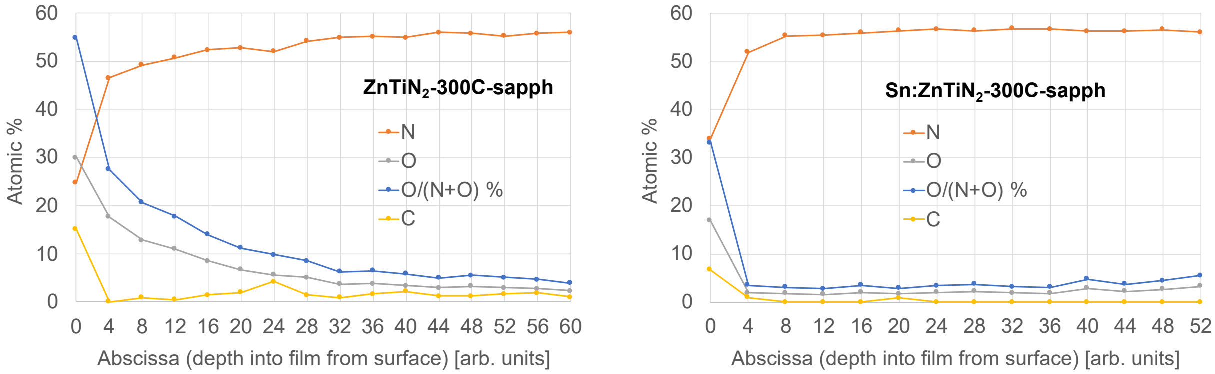

Supplemental Figure 12. XPS depth profiles for nitrogen, oxygen, calculated O/(O+N) %, and carbon for (**left**) $ZnTiN_2$-300C-sapph and (**right**) Sn:$ZnTiN_2$-300C-sapph. The regions used for calculating average O/(O+N) % and C at. % are outlined in green for each film.

Supplemental References

1 S. Ke, J. S. Mangum, A. Zakutayev, A. L. Greenaway and J. B. Neaton, *in preparation*, 2023.
2 A. Jain, S. P. Ong, G. Hautier, W. Chen, W. D. Richards, S. Dacek, S. Cholia, D. Gunter, D. Skinner, G. Ceder and K. A. Persson, *APL Materials*, 2013, **1**, 011002.
3 S. P. Ong, L. Wang, B. Kang and G. Ceder, *Chem. Mater.*, 2008, **20**, 1798–1807.